



City Research Online

City St George's, University of London

Citation: Chen, R., Zhao, T., Wu, W., Wu, F., Li, L., Qian, J., Xu, R., Wu, H., Albishri, H. M., Al-Bogami, A. S., et al (2014). Free-Standing Hierarchically Sandwich-Type Tungsten Disulfide Nanotubes/Graphene Anode for Lithium-Ion Batteries. *Nano Letters*, 14(10), pp. 5899-5904. doi: 10.1021/nl502848z

This is the accepted version of the paper.

This version of the publication may differ from the final published version. To cite this item please consult the publisher's version.

Permanent repository link: <https://openaccess.city.ac.uk/id/eprint/13050/>

Link to published version: <https://doi.org/10.1021/nl502848z>

Copyright and Reuse: Copyright and Moral Rights remain with the author(s) and/or copyright holders. Copies of full items can be used for personal research or study, educational, or not-for-profit purposes without prior permission or charge, unless otherwise indicated, provided that the authors, title and full bibliographic details are credited, a hyperlink and/or URL is given for the original metadata page and the content is not changed in any way. For full details of reuse please refer to [City Research Online policy](#).

Free-standing hierarchically sandwich-type tungsten disulfide nanotubes/graphene anode for lithium-ion batteries

Renjie Chen^{a*||}, Teng Zhao^{||}, Weiping Wu^b, Feng Wu^{a*}, Li Li^a, Ji Qian^a, Rui Xu^c, Huiming Wu^c, Hassan M. Albishri^d, A. S. Al-Bogami^d, Deia Abd El-Hady^d, Jun Lu^{c,*}, Khalil Amine^{c,d,*}.

a Beijing Key Laboratory of Environmental Science and Engineering, School of Chemical Engineering and Environment, Beijing Institute of Technology, Beijing, 100081, China.

B Cambridge Ink Technology Ltd., 91 Devonshire Mews, Devonshire Road, Cambridge, CB1 2BB, United Kingdom

c Chemical Sciences and Engineering Division, Argonne National Laboratory, 9700 South Cass Avenue, Lemont, Illinois 60440, United States

d King Abdulaziz University, Faculty of Science, 80203 Jeddah, Saudi Arabia

ABSTRACT: Transition metal dichalcogenides (TMD), analogue of graphene, could form various dimensionalities. Similar to carbon, one dimensional (1D) nanotube of TMD materials has wide application in hydrogen storage, Li-ion batteries and supercapacitors due to their unique structure and properties. Here we demonstrate the feasibility of tungsten disulfide nanotubes (WS₂-NTs)/graphene (GS) sandwich-type architecture as anode for lithium-ion batteries for the first time. The graphene based hierarchical architecture plays vital roles in achieving fast electron/ion transfer, thus leading to good electrochemical performance. When evaluated as anode, WS₂-NTs/GS hybrid could maintain a capacity of 318.6 mA/g over 500 cycles at a current density of 1A/g. Besides, the hybrid anode does not require any additional polymeric binder, conductive additives or a separate metal current-collector. The relatively high density of this hybrid is beneficial for high capacity per unit volume. Those characteristics make it a potential anode material for light and high performance lithium-ion batteries.

KEYWORDS: Lithium-ion batteries, anode material, graphene, tungsten disulfide nanotube, sandwich-type structure, electro-chemical performance

1
2
3
4 Rechargeable lithium ion batteries (LIBs) have long been considered as the
5 most effective energy-storage technology and dominated portable electronic market
6 for over two decades.^{1,2} Based on the intercalation mechanism, state-of-the-art Li-ion
7 technology can exhibit a theoretical specific energy of ~400 Wh/kg, such as
8 LiCoO₂/graphite system.³ However, it is urgent to explore new chemistries and
9 materials that can significantly increase the cell energy density, considering the future
10 demand for electronic vehicles and large-scale energy storage plants.^{4,5}

11 Graphite, a widely used anode material for the current LIBs, has a theoretical
12 capacity of only 372 mAh/g, given a fully intercalated LiC₆ compound, which is one
13 of the limiting factors for achieving high energy density of the cell⁶. In order to
14 overcome such technical bottleneck, considerable effort has been devoted to design
15 and synthesise new anode materials with higher theoretical specific capacity, such as
16 transition metal oxides (SnO₂, Co₃O₄, Fe₃O₄), Sn and Si⁷. However, all these materials
17 suffer from severe volume variation during charge-discharge cycling, which results in
18 serious pulverisation of the electrodes, and thus, rapid capacity degradation. For
19 instance, Si has a high specific capacity of 4200 mAh/g if fully lithiated to Li_{4.4}Si,
20 however, it also shows a large volume expansion up to 400%. Such volume expansion
21 causes huge mechanical stress of the electrode, and therefore, severely limits the
22 lifetime of Si anode. Although various strategies have been proposed to enhance the
23 structural stability of Si-based materials, including carbon or polymer coating^{8, 9},
24 nano-structuring¹⁰⁻¹² and hierarchical hybridization,¹³⁻¹⁵ it is still very challenge to
25 overcome the issue of the inherent volume change of these materials during cycling.

26 Transition metal dichalcogenides (TMD) MX₂ (M=Mo, Ti, V, and W, X=S or
27 Se)^{16, 17} with the similar feature of layered structure as graphite could have great
28 potential for alternative anode materials. In general, MX₂ has strong covalent bonds
29 within layers and weak Van der Waals forces between layers, which provide ideal
30 space for intercalation of lithium ions. For instance, MoS₂ has much larger spacing
31 between neighboring layers (0.615 nm) than that of graphite (0.335 nm) and weak van
32 der Waals forces between the layers, which, in principal, may make the Li⁺ diffuse
33 easier. However, certain electrochemical properties of MX₂ can only be achieved in
34 their 1-D or 2-D nanostructured crystals because of the relatively high resistance for
35 Li-ion transport in their bulk form. In addition, the electron conductivity of this type
36 of materials is still too low, which could lead to rapid capacity fading and poor rate
37 performance when using as the anode material in a Li-ion cell. A widely used
38 approach to overcome this problem is to design and optimize nanocomposites for
39 good electrical conductivity, since nanostructured TMD likely allows to increase Li-
40 ion intercalation/de-intercalation due to the high surface area and shorter diffusion
41 path for Li-ion transport.

42 Among these TMD compound, MoS₂, as the most studied TMD for Li⁺ storage
43 today, has received considerable attention as a possible anode candidate for Li-ion
44 cells. For instance, MoS₂-C nanotube¹⁸ and graphene/MoS₂ nano-flake¹⁹ have been
45 reported with significant improvement in cycle life and rate performance by taking
46 advantages of the large electrolyte-electrode interface and reduced ion diffuse
47 pathway. On the other hand, WS₂ with higher intrinsic electrical conductivity than
48 MoS₂²⁰, which is not studied in detail yet, could be a more suitable candidate as the
49 anode material for Li-ion cells.

50 Herein, we propose a conceptually new approach to design and fabricate a novel
51 three dimensional WS₂ nanotubes/graphene (WS₂-NTs/GS) hybrid with unique
52 sandwich-type architecture via a simple one-pot hydrothermal reaction. As shown in
53
54
55
56
57
58
59
60

1
2
3 Figure 1, WS₂-NTs/GS hybrid was easily prepared by dispersion WS₂-NTs into
4 homogenous graphene oxide (GO) solution and subsequent hydrothermal reaction at
5 controlled PH value for conversion of GO to GS²¹. GS could curl and cross-link to
6 form 3D network during dehydration due to the combination of hydrophobic nature
7 and π - π interactions²² while WS₂-NT was embedded into the galleries of GS. More
8 importantly, controlling PH of solution by adding appropriate amount of ammonia
9 could further enhance those assemble in a compact manner.²³ The procedure is
10 detailed in the experimental section of the Supporting Information. The unique hybrid
11 could benefit from the synergistic effects of its each component. Specifically, the
12 imbedded WS₂-NTs could effectively prevent GS from complete restacking, thus
13 affording pores and channel for ion diffusion. Meanwhile, the good electrical and
14 mechanical properties of GS could not only enhance the anode conductivity, but also
15 accommodate the volume change of anode during cycling. As a result, WS₂-NTs/GS
16 hybrid exhibited improved cycling stability and rate capability compared with that of
17 WS₂-NTs.
18
19

20
21 X-ray diffraction (XRD) patterns of WS₂-NTs and WS₂-NTs/GS are shown in
22 Figure 2A. The analysis of WS₂-NTs hybrid spectrum shows highly crystalline
23 hexagonal structure (JCPDS No. 84-1398). For WS₂-NTs/GS hybrid, all the
24 diffraction peaks are consistent with that of WS₂-NTs except for an additional small
25 and broad peak appearing at 2θ of 24~26° (inset). Such peak originates from the (002)
26 plane of GS, indicating a disordered stack of graphene sheet. These results suggest
27 that the attachment of WS₂-NTs on GS does not influence its crystallinity and no new
28 phases are generated.
29

30
31 To further elucidate the effect of the deposition of WS₂-NTs on the
32 microstructure of graphene, Raman spectroscopy was carried out to characterize the
33 carbon lattice in the WS₂-NTs/GS hybrid (Figure 2B). The Raman spectrum of pure
34 graphene (GS) showed a pattern of partially graphitized carbon. The peak at ~1350
35 cm⁻¹ (D band) is assigned to defects and disorder in the graphene layer while peaks at
36 ~1593 cm⁻¹ (G band) is related to the coplanar vibration of sp²-bonded carbon atoms
37 in GS. Interestingly, the intensity of the D band in the WS₂-NTs/GS hybrid is higher
38 than that of the pure GS, indicating a more disordered stack of graphene layer in the
39 hybrid. To some extents, it reveals that the WS₂-NTs were embedded into the
40 interlayer galleries of GS and prevent it from restacking. It should also be noted that
41 the characteristic Raman scattering peaks for WS₂-NTs are mainly observed below
42 1000 cm⁻¹, which is consistent with the crystalline nature of WS₂-NTs in the hybrid.²⁴
43
44

45 To determine the chemical composition of WS₂-NTs/GS hybrid, X-ray
46 photoelectron spectroscopy (XPS) analyses were conducted. According to the broad
47 XPS scan spectrum in the region of 0-1100 eV (Figure 3A), four elements including
48 W, S, C, O are detected and their atomic concentration is 7.55%-W, 13.54%-S,
49 66.91%-C, 12.00%-O, respectively. The calculated atomic ratio of S to W is ~1.8,
50 closed to the theoretically predicted value for WS₂. The W_{4f}XPS spectra of the hybrid
51 exhibits peaks observed at 33.5 eV and 31.3 eV, corresponding to the W_{4f5/2} and W_{4f7/2}
52 characteristic peaks of WS₂-NTs (Figure 3B). As for the peak at 36.9 eV, we assign it
53 to the W-O bond, indicating a low surface oxidation²⁵. The presence of WS₂-NTs can
54 be further confirmed by the two distinct S_{2p} peaks at 161.9 eV and 163.2 eV, which
55 correspond to the S_{2p3/2} and S_{2p1/2} components of WS₂-NTs (Figure 3C). Besides, C1s
56 (284.5eV) and O1s (530eV) peaks are mainly attributed to the carbon and oxygen
57
58
59
60

1
2
3 atom in GS. The deconvolution of the C1s peaks is displayed in Figure 3D. Peaks
4 centred at 286.1, 287.9 eV are attributed to the residual C-O and C=O groups,
5 respectively. Compared with the case of GO²⁶, the peak intensities of most oxygen
6 containing groups decrease remarkably, indicating the restoration of sp² hybridized
7 carbon network. Meanwhile, the O/C ratio was 1:5.6 for the hybrid, which was also
8 consistent with the reduction degree of GO by dehydration mechanism²⁷.
9 Accordingly, we can conclude that the hybrid consists of GS and WS₂-NTs, whose
10 content are about 35.4 wt % and 64.6 wt%, respectively.
11

12
13 The morphology and structure of the WS₂-NTs/GS hybrid were characterized by
14 SEM and TEM. The SEM image (Figure 4A) of WS₂-NTs exhibits a uniform one
15 dimensional (1D) structure with diameter of around 60 nm and length of about 5 μ m.
16 Like carbon nanotubes, such straight structure could easily form bundles, which
17 provide extra lithium intercalation between inter-tubular sites. Figure 4B shows the
18 electron diffraction pattern of two parallel WS₂-NTs. The {10 $\bar{1}$ 0} spots appear to be
19 arranged in a double-hexagonal pattern, corresponding to in plane diffractions in each
20 tube²⁸. The HR-TEM image (Figure 4C) of individual WS₂-NTs clearly displays the
21 hollow interior and multi-walls. Compared with straight WS₂-NTs, WS₂-NTs/GS
22 hybrid display a three dimensional (3D) sandwich-like architecture that individual
23 WS₂ nanotubes are homogeneously incorporated into the interlayer galleries of
24 graphene sheets (Figure 4D). From the magnified SEM (inset), we can see that thin
25 graphene could easily wrap around WS₂-NTs due to its flexibility. The
26 microstructure of WS₂-NTs/GS hybrid was further analyzed by HR-TEM (Figure 4D
27 and 4E). It is clear that WS₂-NTs bundles were well dispersed in graphene matrices.
28 According to the cross-sectional images, there are about five layer graphene sheets
29 wrapping around the edges of WS₂-NTs, which have a d-spacing of approximately
30 0.62 nm twice than that of GS (~0.34 nm). Figure 4G shows the photograph of the
31 black cylinder of the assembled WS₂-NTs/GS hybrid, which can be cut and
32 compressed into circular pellet with a diameter of 11 mm for direct use as anode in
33 standard CR 2025 coin cell.
34
35
36

37 To investigate the anode performance of the WS₂-NTs/GS hybrid,
38 electrochemical characterization was conducted based on two-electrode coin-type
39 cells (CR 2025) with Li metal as the counter-electrode. Figure 5A shows cyclic
40 voltammograms (CV) of the WS₂-NTs/GS hybrid anode for the initial three cycles
41 between 0.01 and 3.00 V at a scan rate of 0.1 mV/s. In the first cycles, two small
42 cathodic peaks at 1.6 V and 1.5 V are observed, which correspond to the lithium
43 insertion to WS₂ to form Li_xWS₂. The following sharp overlap peak at 0.75 V could
44 be attributed to the subsequent conversion reaction of Li with WS₂ and the formation
45 of a solid electrolyte interlayer (SEI)^{29, 30}. The starting cathodic peak at 0.5 V is
46 related to the insertion of Li⁺ into graphene, which is also electroactive for lithium
47 storage³¹. During the anodic scan, three oxidation peaks at 1.0, 1.6, 2.2 V are
48 observed, corresponding to the reverse extraction of Li⁺ from graphene and Li_xWS₂
49 host, respectively. From the second cycle onward, the cathodic peak at 0.75 V
50 disappears while the original cathodic peaks at 1.6 V and 1.5 V shift to 2.1 V and 1.8
51 V, indicating improved reversibility of lithiation and delithiation with cycling. In
52 addition, no obvious changes are observed for the redox peaks, implying that the
53 anode exhibits good electrochemical stability. For comparison, the CV of just WS₂-
54 NTs is shown in Figure S1. It can be seen that the electrochemical behavior of WS₂-
55 NTs is almost the same with that of WS₂-NTs/GS hybrid except the absence of redox
56
57
58
59
60

1
2
3 related to the insertion/extraction of Li^+ into/from GS.
4

5 Figure 5B shows the galvanostatic charge/discharge profiles of the WS_2 -NTs/
6 GS hybrid anode in the 1st, 2nd, 10th and 50th at a current density of 0.1 A/g. The
7 hybrid anode delivers an initial capacity of 996.4 mAh/g and a corresponding charge
8 capacity of 697.7 mAh/g with a first-cycle Coulombic efficiency of $\sim 70.0\%$. The
9 large discharge capacity is attributed to the formation of SEI layer and the irreversible
10 conversion reaction between Li and WS_2 , which are consistent with the above CV
11 analysis. After the initial capacity loss, a high capacity retention upon cycling are
12 observed and the pattern of discharge and charge plateaus remains unchanged. A
13 capacity of 500.2 mAh/g is achieved after 50 cycles. For comparison, pure WS_2 -NTs
14 were tested under the same current density as that for the WS_2 -NTs/GS hybrid anode
15 (Figure S2). The first discharge and charge capacities for WS_2 -NTs anode are 768.5
16 and 660.8 mAh/g, respectively. And serious capacity decay is observed with cycling,
17 accompanied with the gradual disappearance of discharge plateaus at ~ 2.0 V. After 50
18 cycles, the capacity of WS_2 -NTs anode dramatically decreases to 202.8 mAh/g.
19

20
21 Figure 5C reveals tenth-cycle discharge capacities of around 692.6, 574.8, 546.2,
22 393.5 mAh/g at current density of 0.1, 0.2, 0.5, 1.0 A/g, respectively. Besides, the
23 specific capacity of WS_2 -NTs/GS hybrid anode could recover to 487.9 mAh/g when
24 the current density is returned to 0.1 A/g. More importantly, the galvanostatic
25 measurements for the WS_2 -NTs/GS hybrid anode at increasing rate (inset) show the
26 same pattern of discharge and charge plateaus, indicating good rate performance and
27 rate tolerance. In contrast, pure WS_2 -NTs anode exhibits poor capacities and rate
28 capabilities. Even when the current density reduced, the capacity cannot recover its
29 initial level. This difference supports that the 3D hierarchical structure could
30 successfully enhance electronic/ionic transport within the anode, resulting improved
31 electrochemical kinetics, which is further evidenced by the results of EIS (Figure 5D)
32 that the charge-transfer resistance (R_{ct}) values of WS_2 -NTs/GS hybrid anode is found
33 to be 37.5 Ω , which is lower than that of WS_2 -NTs (52.6 Ω).
34
35

36
37 Figure 5E compares the long cycle performance of WS_2 -NTs and WS_2 -NTs/GS
38 hybrid anode at high current density of 1 A/g. In the case of WS_2 -NTs/GS hybrid
39 anode, the initial capacity is as high as 886.1 mAh/g and it still maintains a capacity
40 of 318.6 mAh/g after 500 cycles. In contrast, much more capacity decay is observed
41 for WS_2 -NTs. The specific capacity dramatically decreases from 695.4 mAh/g to
42 171.9 mAh/g after 500 cycles. The good cycle performance of WS_2 -NTs/GS hybrid
43 anode benefits from the following factors: (1) the incorporation of GS significantly
44 enhances the conductivity of anode; (2) the hybrid 3D architecture consisting of
45 layered WS_2 -NTs and GS affords pores and large electrolyte/electrode interface, thus
46 providing channels for Li-ion diffusion and reactive sites for Li-ion intercalation; (3)
47 the flexible GS could effectively accommodate the volume change during cycling.
48
49

50 In summary, we have demonstrated the feasibility of WS_2 nanotube/graphene
51 sandwich-type architecture for good electrochemical performance. To the best of our
52 knowledge, it is the first time for reporting such a conceptual design. Compared with
53 pure WS_2 -NTs, the hybrid anode exhibits much improved cycling stability and rate
54 capability without additional polymeric binder, conductive additives or a separate
55 metal current-collector. More importantly, the relatively high density of this hybrid is
56 beneficial for high capacity per unit volume, which offsets its poor operating potential and
57 thus makes it a promising anode material for light and high performance lithium-ion
58
59
60

1
2
3 batteries.

4
5 ASSOCIATED CONTENT

6
7 Supporting Information

8
9 Detail of experimental and additional figures depicting experiment results. This
10 material is available free of charge via the Internet at <http://pubs.acs.org>.

11
12
13
14 AUTHOR INFORMATION

15
16 Corresponding Author

17 *E-mail: chenrj@bit.edu.cn, wufeng863@vip.sina.com, junlu@anl.gov and
18 amine@anl.gov

19
20 Author Contribution

21
22 ||R.C. and T.Z. contributed equally to this work.

23
24 Notes

25
26 The authors declare no competing financial interest.

27
28
29
30 ACKNOWLEDGMENT

31
32 This work was supported by the National Science Foundation of China (NSFC,
33 21373028), the National 863 Program (2011AA11A256), New Century Educational
34 Talents Plan of Chinese Education Ministry (NCET-12-0050) and Beijing Nova
35 Program (Z121103002512029). This work was also supported by the U.S.
36 Department of Energy under Contract DE-AC0206CH11357 from the Vehicle
37 Technologies Office, Department of Energy, Office of Energy Efficiency and
38 Renewable Energy (EERE) and Division of Materials Science, Basic Energy
39 Sciences, Department of Energy, Office of Science. Argonne National Laboratory, a
40 U.S. Department of Energy Office of Science laboratory, is operated under Contract
41 No. DE-AC02-06CH11357. This project was also funded by the Deanship of
42 Scientific research (DSR), King Abdulaziz University, Jeddah under the HiCi
43 Project(grant No: 11-130-1434HiCi). The authors (HMA, DAE, ASA and KA) thank
44 the DSR for their technical and financial support. The authors also acknowledge the
45 U.S.-China Electric Vehicle and Battery Technology Collaboration between Argonne
46 National Laboratory and Beijing Institute of Technology.

47
48
49
50 References

- 51
52
53
54
55
56
57
58
59
60
1. Armand, M.; Tarascon, J. M. *Nature* **2008**, *451*, 652-657.
 2. Scrosati, B.; Garche, J. J. *Power Sources* **2010**, *195*, 2419-2430.
 3. Kang, B.; Ceder, G. *Nature* **2009**, *458*, 190-193.
 4. Tarascon, J. M.; Armand, M. *Nature* **2001**, *414*, 359-367.
 5. Dunn, B.; Kamath, H.; Tarascon, J.-M. *Science* **2011**, *334*, 928-935.

6. Wu, Y. P.; Rahm, E.; Holze, R. *J. Power Sources* **2003**, *114*, 228-236.
7. Tirado, J. L. *Mat. Sci. Eng. R* **2003**, *40*, 103-136.
8. Wang, C.; Wu, H.; Chen, Z.; McDowell, M. T.; Cui, Y.; Bao, Z. *Nat. Chem.* **2013**, *5*, 1042-1048.
9. Chen, Z.; Zhou, M.; Cao, Y.; Ai, X.; Yang, H.; Liu, J. *Adv. Energy Mater.* **2012**, *2*, 95-102.
10. Bruce, P. G.; Scrosati, B.; Tarascon, J.-M. *Angew. Chem. Int. Ed.* **2008**, *47*, 2930-2946.
11. Chan, C. K.; Peng, H.; Liu, G.; McIlwrath, K.; Zhang, X. F.; Huggins, R. A.; Cui, Y. *Nat. Nanotechnol.* **2008**, *3*, 31-35.
12. Arico, A. S.; Bruce, P.; Scrosati, B.; Tarascon, J.-M.; van Schalkwijk, W. *Nat. Mater.* **2005**, *4*, 366-377.
13. Magasinski, A.; Dixon, P.; Hertzberg, B.; Kvit, A.; Ayala, J.; Yushin, G. *Nat. Mater.* **2010**, *9*, 353-358.
14. Zhou, G.; Wang, D.-W.; Li, F.; Zhang, L.; Li, N.; Wu, Z.-S.; Wen, L.; Lu, G. Q.; Cheng, H.-M. *Chem. Mater.* **2010**, *22*, 5306-5313.
15. Wang, H.; Cui, L.-F.; Yang, Y.; Sanchez Casalongue, H.; Robinson, J. T.; Liang, Y.; Cui, Y.; Dai, H. *J. Am. Chem. Soc.* **2010**, *132*, 13978-13980.
16. Ghorbani-Asl, M.; Zibouche, N.; Wahiduzzaman, M.; Oliveira, A. F.; Kuc, A.; Heine, T. *Sci. Rep.* **2013**, *3*, 2961.
17. Zak, A.; Feldman, Y.; Lyakhovitskaya, V.; Leitus, G.; Popovitz-Biro, R.; Wachtel, E.; Cohen, H.; Reich, S.; Tenne, R. *J. Am. Chem. Soc.* **2002**, *124*, 4747-4758.
18. Zhang, C.; Wang, Z.; Guo, Z.; Lou, X. W. *ACS Appl. Mater. Inter.* **2012**, *4*, 3765-3768.
19. Yu, H.; Ma, C.; Ge, B.; Chen, Y.; Xu, Z.; Zhu, C.; Li, C.; Ouyang, Q.; Gao, P.; Li, J.; Sun, C.; Qi, L.; Wang, Y.; Li, F. *Chem.-Eur. J.* **2013**, *19*, 5818-5823.
20. Zhang, C.; Ning, Z.; Liu, Y.; Xu, T.; Guo, Y.; Zak, A.; Zhang, Z.; Wang, S.; Tenne, R.; Chen, Q. *Appl. Phys. Lett.* **2012**, *101*, 113112.
21. Xu, Y.; Sheng, K.; Li, C.; Shi, G. *ACS Nano* **2010**, *4*, 4324-4330.
22. Zhou, G.; Yin, L. C.; Wang, D. W.; Li, L.; Pei, S.; Gentle, I. R.; Li, F.; Cheng, H. M. *ACS Nano* **2013**, *7*, 5367-5375.
23. Bi, H.; Yin, K.; Xie, X.; Zhou, Y.; Wan, N.; Xu, F.; Banhart, F.; Sun, L.; Ruoff, R. S. *Adv. Mater.* **2012**, *24*, 5124-5129.
24. Krause, M.; Virsek, M.; Remškar, M.; Kolitsch, A.; Möller, W. *Phys. Status Solidi B* **2009**, *246*, 2786-2789.
25. Ratha, S.; Rout, C. S. *Acs Applied Materials & Interfaces* **2013**, *5*, 11427-11433.
26. Dreyer, D. R.; Park, S.; Bielawski, C. W.; Ruoff, R. S. *Chem. Soc. Rev.* **2010**, *39*, 228-240.
27. Liao, K. H.; Mittal, A.; Bose, S.; Leighton, C. S.; Mkhoyan, K. A.; Macosko, C. M. *ACS Nano* **2011**, *5*, 1253-1258.
28. Whitby, R. L. D.; Hsu, W. K.; Fearon, P. K.; Billingham, N. C.; Maurin, I.; Kroto, H. W.; Walton, D. R. M.; Boothroyd, C. B.; Firth, S.; Clark, R. J. H.; Collison, D. *Chem. Mater.* **2002**, *14*, 2209-2217.
29. Liu, H.; Su, D.; Wang, G.; Qiao, S. Z. *J. Mater. Chem.* **2012**, *22*, 17437-17440.
30. Wang, S.; Li, G.; Du, G.; Li, L.; Jiang, X.; Feng, C.; Guo, Z.; Kim, S. *Nanoscale Res. Lett.* **2010**, *5*, 1301-1306.
31. Wang, G.; Shen, X.; Yao, J.; Park, J. *Carbon* **2009**, *47*, 2049-2053.

1
2
3 Figure Captions:

4 Figure 1. Schematic illustration of the fabrication of 3D hierarchically structured
5 WS₂-NT/GS hybrid.
6

7 Figure 2. (A) XRD patterns of WS₂-NTs and WS₂-NTs/GS hybrid; (B) Raman spectra
8 of WS₂-NTs/GS hybrid with those of WS₂-NT and GS.
9

10 Figure 3. XPS spectra of WS₂-NTs/GS hybrid: (A) broad scan spectrum; (B) W4f; (C)
11 S2p; (D) C1s.

12 Figure 4. (A) and (D) SEM images of WS₂-NTs and WS₂-NTs/GS hybrid; (B) and (C)
13 HR-TEM images of WS₂-NTs; (E) and (F) HR-TEM images of WS₂-NTs/GS hybrid;
14 (G) photography of WS₂-NTs/GS hybrid and schematic illustration of the fabrication
15 WS₂-NTs/GS anode in standard CR 2025 coin cell.
16
17

18 Figure 5. (A) Cyclic voltammetry of the WS₂-NTs/GS hybrid anode over a voltage
19 range of 0.01–3.00 V at a scanning rate of 0.1 mV/s; (B) Discharge/charge voltage
20 profiles of WS₂-NTs/GS hybrid anode at a current density of 100 mA/g; (C) rate
21 capabilities of WS₂-NTs/GS hybrid and WS₂-NTs anode, inset: discharge/charge
22 voltage profiles of WS₂-NTs/GS hybrid at current density of 0.1, 0.2, 0.5, 1 A/g; (D)
23 Nyquist plots of the WS₂-NTs/GS hybrid and WS₂-NTs anode at open potential before
24 cycling; (E) Cycling stability of WS₂-NTs/GS hybrid and WS₂-NTs anode at 1 A /g
25 for 500 cycles.
26
27
28
29
30
31
32
33
34
35
36
37
38
39
40
41
42
43
44
45
46
47
48
49
50
51
52
53
54
55
56
57
58
59
60

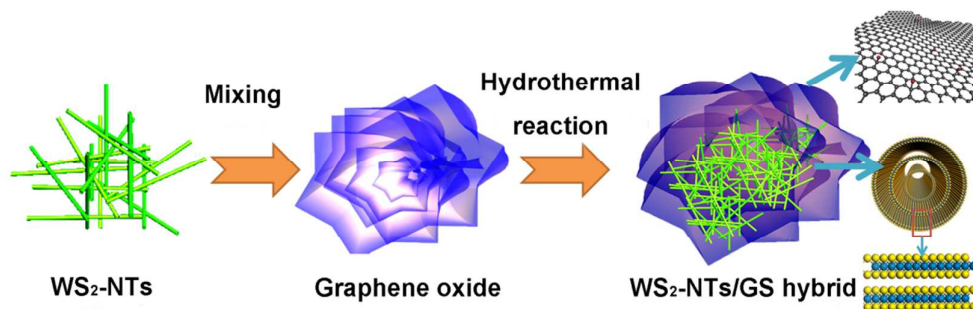


Figure 1. Schematic illustration of the fabrication of 3D hierarchically structured WS₂-NT/GS hybrid.

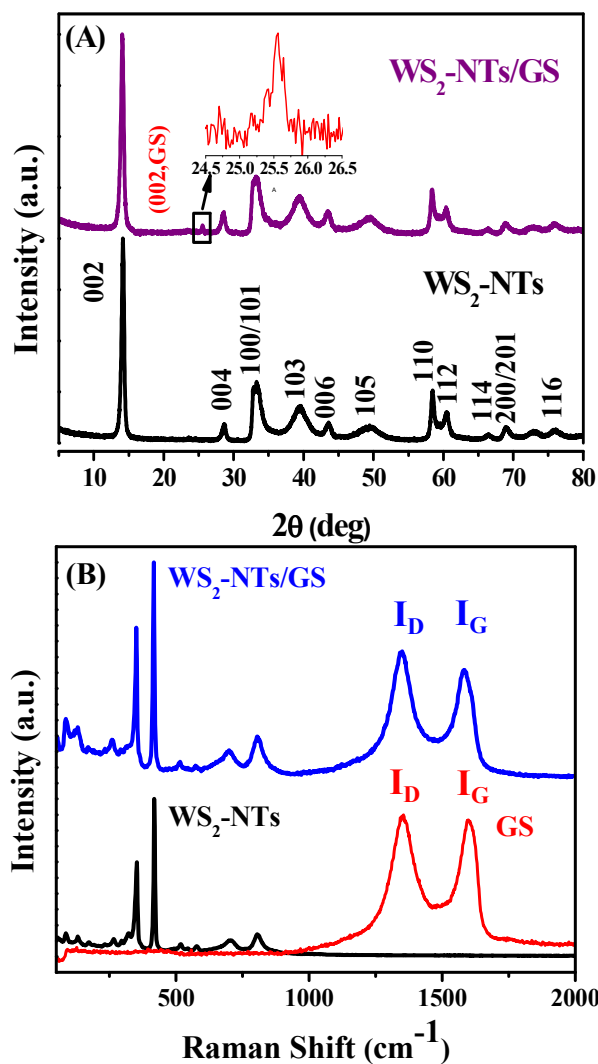


Figure 2. (A) XRD patterns of WS₂-NTs and WS₂-NTs/GS hybrid; (B) Raman spectra of WS₂-NTs/GS hybrid with those of WS₂-NT and GS.

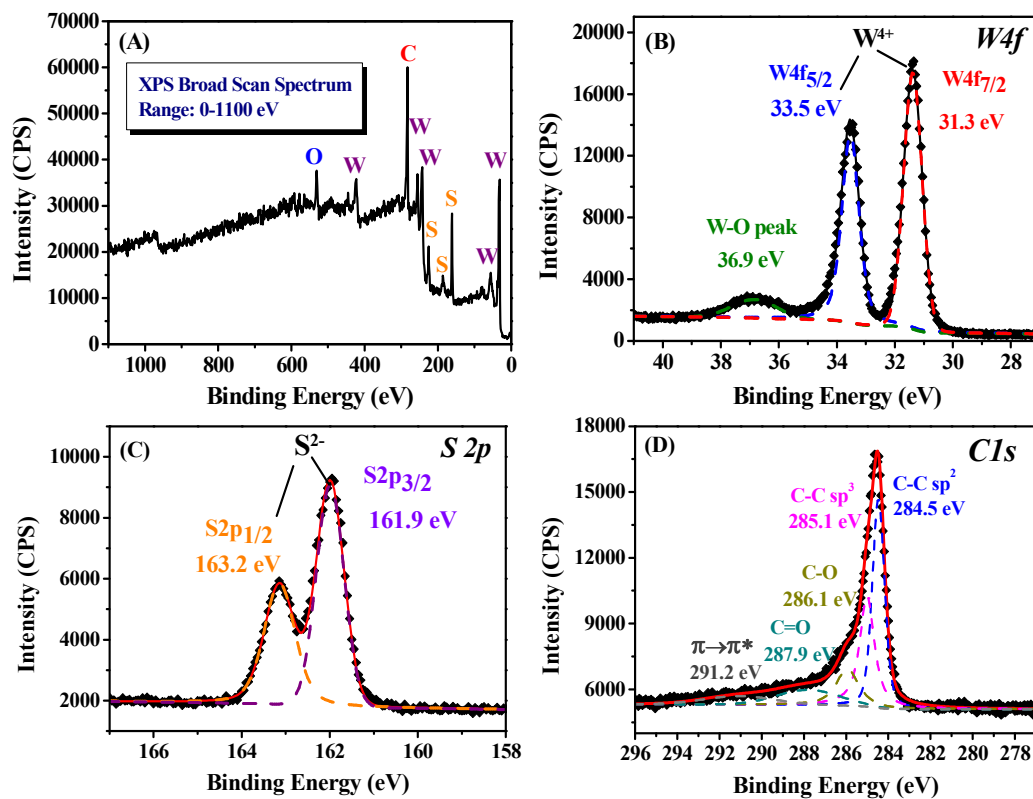


Figure 3. XPS spectra of WS₂-NTs/GS hybrid: (A) broad scan spectrum; (B) W4f; (C) S2p; (D) C1s.

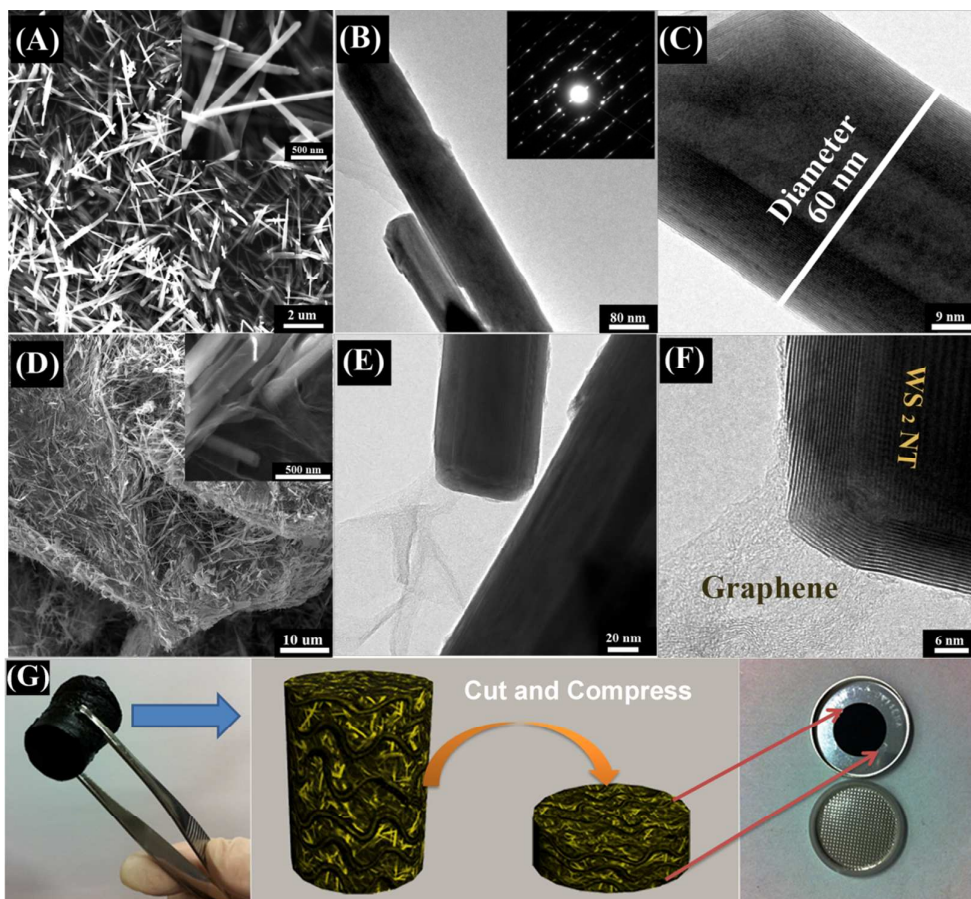


Figure 4. (A) and (D) SEM images of WS₂-NTs and WS₂-NTs/GS hybrid; (B) and (C) HR-TEM images of WS₂-NTs; (E) and (F) HR-TEM images of WS₂-NTs/GS hybrid; (G) photography of WS₂-NTs/GS hybrid and schematic illustration of the fabrication WS₂-NTs/GS anode in standard CR 2025 coin cell.

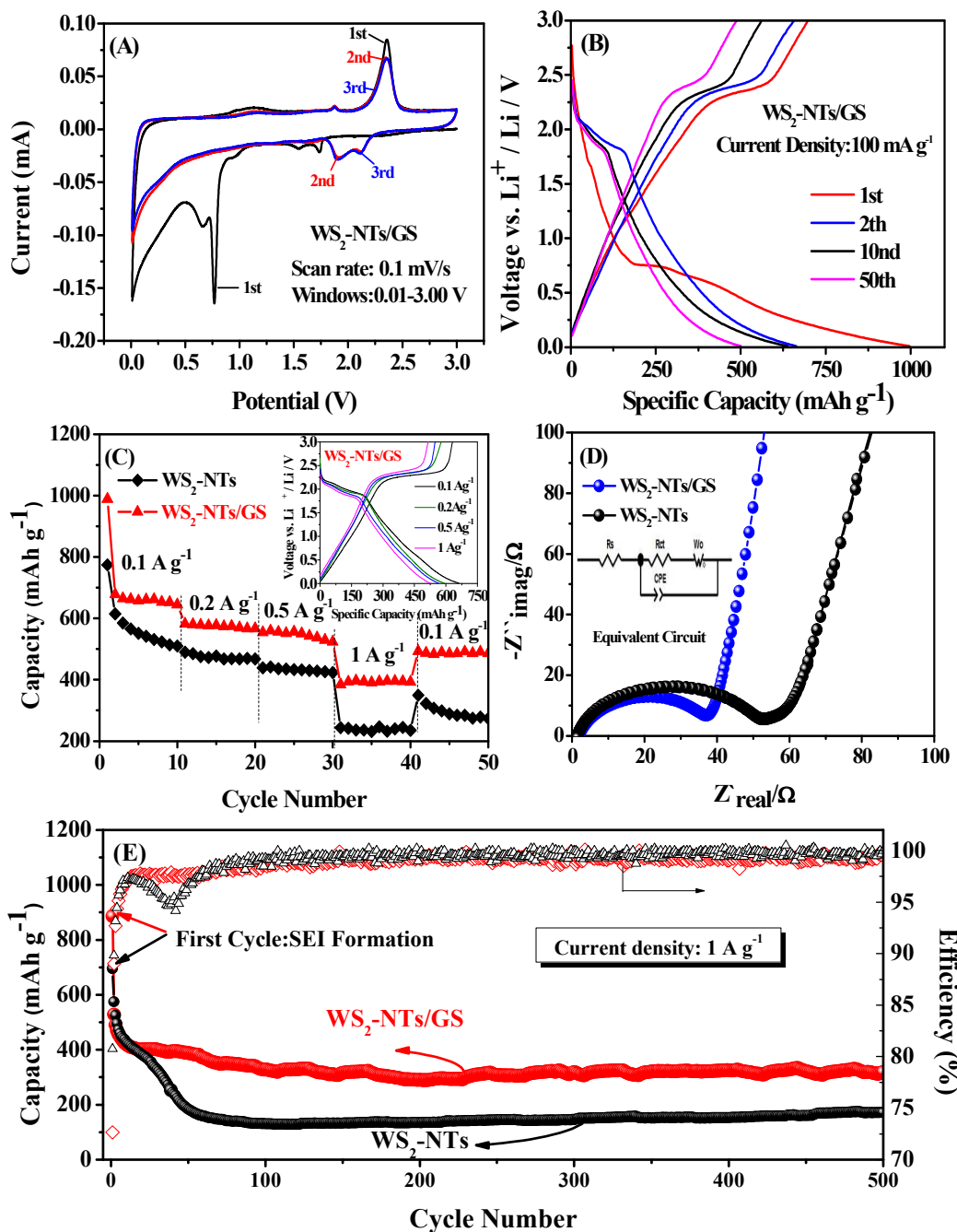
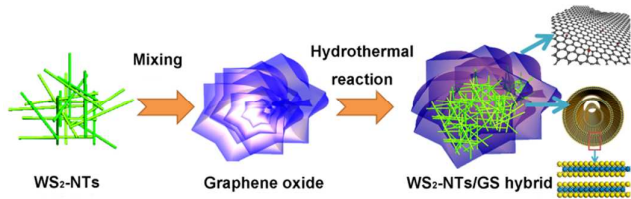


Figure 5 (A) Cyclic voltammety of the WS₂-NTs/GS hybrid anode over a voltage range of 0.01–3.00 V at a scanning rate of 0.1 mV/s; (B) Discharge/charge voltage profiles of WS₂-NTs/GS hybrid anode at a current density of 100 mA/g; (C) rate capabilities of WS₂-NTs/GS hybrid and WS₂-NTs anode, inset: discharge/charge voltage profiles of WS₂-NTs/GS hybrid at current density of 0.1, 0.2, 0.5, 1 A/g; (D) Nyquist plots of the WS₂-NTs/GS hybrid and WS₂-NTs anode at open potential before cycling; (E) Cycling stability of WS₂-NTs/GS hybrid and WS₂-NTs anode at 1 A/g for 500 cycles.

TOC



1
2
3
4
5
6
7
8
9
10
11
12
13
14
15
16
17
18
19
20
21
22
23
24
25
26
27
28
29
30
31
32
33
34
35
36
37
38
39
40
41
42
43
44
45
46
47
48
49
50
51
52
53
54
55
56
57
58
59
60